Nonlin. Processes Geophys., 17, 715–731, 2010
www.nonlin-processes-geophys.net/17/715/2010/
doi:10.5194/npg-17-715-2010

Nonlinear Processes in Geophysics

Inhomogeneous dominance patterns of competing phytoplankton groups in the wake of an island

D. Bastine and U. Feudel

Institute for Chemistry and Biology of the Marine Environment, Theoretical Physics/Complex Systems, Carl von Ossietzky University Oldenburg, Germany

Received: 15 June 2010 – Revised: 20 October 2010 – Accepted: 25 November 2010 – Published: 8 December 2010

Abstract. We investigate the competition between two different functional groups of phytoplankton in the wake of an island close to a coastal upwelling region. We couple a simple biological model with three trophic levels and a hydrodynamic model of a von Kármán vortex street. The spatio-temporal abundance shows that the different phytoplankton groups dominate in different regions of the flow. The composition of the phytoplankton community varies e.g. for the different vortices. We study the mechanism leading to these inhomogeneous dominance patterns by investigating the nutrient transport in the flow and the interplay of hydrodynamic and biological time scales.

1 Introduction

Hydrodynamic motion has a strong influence on the dynamics of plankton populations living in the marine environment. This impact has recently been investigated in numerous studies (Denman and Gargett, 1995; Abraham, 1998; López et al., 2001; Martin, 2003; Tél et al., 2005; Sandulescu et al., 2007, 2008; Rossi et al., 2008; Maraldi et al., 2009). Horizontal transport through mesoscale hydrodynamic structures such as vortices leads to a redistribution of nutrients and plankton and can cause several interesting phenomena (Abraham, 1998; López et al., 2001; Martin and Pondaven, 2003; Tél et al., 2005; Sandulescu et al., 2007, 2008; Rossi et al., 2008; Maraldi et al., 2009; Bracco et al., 2009). A very important role in understanding these phenomena is played by the interplay of hydrodynamic and biological time scales (Abraham, 1998; Richards and Brentnall, 2006; Sandulescu et al., 2007; McKiver et al., 2009; Pérez-Muñuzuri and Huhn, 2010). By modeling plankton growth in a simplified model for turbulent advection Abraham (1998) showed that this interplay can help to explain the patchiness of plankton distributions observed in the ocean. McKiver et al. (2009) and McKiver and Neufeld (2009) showed that small changes in the ratio of biological and hydrodynamic time scales can greatly enhance or reduce the global plankton productivity. Thus, horizontal mixing is a possible trigger of plankton blooms in the ocean. Because the biological activity depends strongly on the availability of nutrients, the vertical transport of these nutrients also has a very strong impact (Denman and Gargett, 1995; Martin and Pondaven, 2003; Perruche et al., 2010). Localized upwelling regions transport nutrient rich water from deeper layers into the euphotic zone where it strongly influences the dynamics of the plankton populations.

There are several places on earth where both vertical upwelling and mesoscale structures occur together. One example studied in Sandulescu et al. (2006, 2007, 2008) is the Canary archipelago with upwelling regions near the African coast and mesoscale vortices in the wake of the islands (Aristegui et al., 1997). The interplay of these mesoscale hydrodynamic structures and plankton dynamics can give rise to several phenomena such as localized (Sandulescu et al., 2007, 2008) or sustained (Hernández-García and López, 2004) plankton blooms. Sandulescu et al. (2007) found a possible mechanism responsible for localized plankton blooms in these vortices, emerging in the wake of an island, using a simplified hydrodynamic and biological model. They focused on the evolution of one species in a simplified model flow finding that the interplay of hydrodynamic and biological time scales is the most important factor for this bloom to appear (Sandulescu et al., 2008). An interesting question is how different species interact in these mesoscale vortices which are connected with the near upwelling region.

The interaction of different species in mesoscale structures has been addressed in Bracco et al. (2000); Károlyi et al. (2000); Scheuring et al. (2003); Tél et al. (2005); Richards

Correspondence to: D. Bastine
(david.bastine@uni-oldenburg.de)

and Brentnall (2006). In particular Bracco et al. (2000); Károlyi et al. (2000); Scheuring et al. (2003) found that these structures can enhance biodiversity, i.e. the coexistence of different species. The hydrodynamic motion leads to an incomplete mixing which allows for a spatial separation of species protecting the less fit species from competition. Taking the finite size of species into account Benczik et al. (2003, 2006) found that a spatial separation can also be caused by a different inertia of species. These different physical properties lead to an accumulation of the different species in different parts of the flow preventing them from competing. These works however did not take the transport of nutrients into account which obviously plays an essential role. Furthermore, they focused on strongly simplified biological models, e.g. not taking zooplankton and hence grazing predators into account.

In this work we investigate an extension of the coupled model studied in Sandulescu et al. (2007, 2008). Instead of using a three trophic level food chain to describe the plankton dynamics we investigate the behavior of a simple food web. This is done by dividing the phytoplankton into two different functional groups which are characterized by different growth rates. This way we are able to address the question of competition of two phytoplankton groups for the same nutrients. We study the behavior of this biological model coupled to a simplified model of the von Kármán vortex street in the wake of an island. The aim of this paper is to show that the transport of nutrients by the vortices in the wake of an island and the interplay of biological processes with the mesoscale hydrodynamic structures allows an inhomogeneous distribution of the different phytoplankton groups in such a way that the different phytoplankton groups dominate the phytoplankton community in different regions of the flow. The composition of the phytoplankton community can vary for vortices differing by position and sign of vorticity. Furthermore, the composition varies even among different regions of a single vortex. Additionally, we show that the effect of diffusion plays an important role for the composition of the phytoplankton community in the mesoscale structures of the flow due to its impact on the competition.

The organization of the paper is as follows: in the first section we introduce the hydrodynamic as well as the biological model under investigation. The observation region in the wake of an island and the velocity field which models the von Kármán vortex street are described. This is followed by a short description of the predator prey model with competing phytoplankton groups and its behavior without taking hydrodynamic motion into account.

In Sect. 3 we present the results of simulations coupling hydrodynamic motion and biological model. The observed spatial and temporal patterns of the different phytoplankton groups are described phenomenologically. Afterwards, we discuss the mechanism leading to these observed patterns by investigating the hydrodynamic transport and the interplay of biological and hydrodynamic time scales.

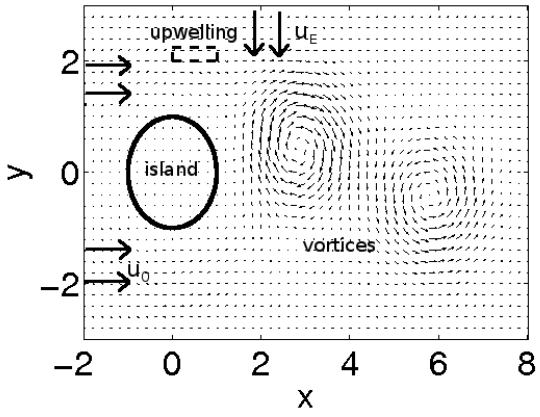

Fig. 1. A sketch of the observation region with the model velocity field (black arrows). The spatial coordinates are given in units of the island radius $r = 25\,\mathrm{km}$. The upwelling region is located at $[0,1] \times [2, 2.25]$. Two vortices with vortex strength ω can be seen in the island wake. The mean velocity field u_0 points in the positive x-direction, while the Ekman flow u_E, existing for $x > 1$, points in the negative y-direction.

A discussion of our results and their implication for marine ecological systems can be found in the last section.

2 Modeling framework

In this section we present the modeling framework used in this work. We begin with briefly explaining the hydrodynamic model of a wake of an island, which is based on a two-dimensional stream function. Afterwards, the biological model is described and first results on the interaction of the two phytoplankton groups are presented without taking hydrodynamic motion into account. This is followed by a description of the coupled model combining the two former presented models.

2.1 Hydrodynamic model: the von Kármán vortex street

The 2-D hydrodynamic model describes the horizontal flow around an island and vortices in its wake (Fig. 1). Water is flowing into the observation region at the left boundary with a velocity u_0. The interaction of the flow with the island leads to a non-stationary velocity field which can be exactly described by the Navier-Stokes equations and corresponding boundary conditions. For a particular range of Reynolds numbers the flow is determined by a periodic detachment of vortices which then travel in the main flow direction (Jung et al., 1993). Jung et al. (1993) introduced a time periodic stream function whose corresponding velocity field shows an astonishing qualitative agreement with the flow from direct numerical simulations of the Navier-Stokes equations. We use an extended version of this model flow

including an Ekman drift perpendicular to the main flow introduced by Sandulescu et al. (2006).

The model stream function yields a two-dimensional velocity field:

$$u(x,y,t) = \partial_y \Psi \quad v(x,y,t) = -\partial_x \Psi \ . \tag{1}$$

The velocity field given by Eq. (1) can be interpreted as a Hamiltonian system with one degree of freedom (Tél et al., 2005). The time dependence leads to chaotic behavior of tracers although the flow field itself is laminar. Since there is a net current through the observation region such a field is referred to as an open chaotic flow in the literature. Tél et al. (2005) showed the existence of a chaotic saddle in the vicinity of the island. This chaotic saddle is given by the union of all non-escaping orbits of tracers in the flow. Although this chaotic saddle is of measure zero its unstable and stable manifolds have a strong influence on the flow of tracers which will be important when investigating the hydrodynamic transport in Sect. 3.2.1.

The usage of a two-dimensional model is justified by the assumption that we have a well mixed upper layer and only small mean vertical velocities compared to the horizontal ones. The exact form and a detailed discussion of the single terms of the stream function $\Psi(x,y,t)$ can be found in Sandulescu et al. (2006). Here we focus on a simple qualitative description which introduces all parameters important to this work.

The stream function is periodic with a period length of T_c. Vortices are created behind the island with a phase difference of half a period $\frac{T_c}{2}$. At maximum two vortices are traveling in the direction of the main flow. These two vortices differ in their signs of vorticity and their position (Fig. 1). In the following we will refer to them as the lower vortex which is located below the center of the island and has a positive vorticity and as the upper vortex which is located above the center of the island and has a negative vorticity. The upper boundary of the observation area corresponds to the African coast line.Another important parameter is the vortex strength ω which determines the magnitude of vorticity and thus the velocities in the vortices. The Ekman flow u_{E} points in the negative y-direction with a constant magnitude but only occurring in the island wake.

The model has been parameterized in Sandulescu et al. (2006) for the region of the Canary islands (Table 1). Using this set of parameters we make sure that we are dealing with a hydrodynamic flow in a realistic order of magnitude.

2.2 Biological model: a food web with three trophic levels

The biological model used in this work is based on a three component NPZ-model (N..Nutrients, P..Phytoplankton, Z..Zooplankton) originally developed by Steele and Henderson (1981) and later modified by Edwards and Brindley (1996) and Pasquero et al. (2005). Since we are interested in the interplay of mesoscale hydrodynamic motion and the competition of species we extend the model of Pasquero et al. (2005) by dividing phytoplankton P into two functional groups of phytoplankton species. We do this division by a simple additive formulation for the consumption terms of nutrients and for the growth terms of zooplankton. This linear combination is one of the standard formulations for these kinds of models (see e.g. Grover, 1997) but of course there are other formulations in the literature as well (Beddington, 1975; Deangelis et al., 1975; Pal et al., 2009) which work with more complex functional responses. We expect that these more complex formulations lead to even more complex behavior which would also be interesting to explore. However, to concentrate on the interplay of the biological model and the hydrodynamic flow we choose a biological model with a less complex behavior. The extended model is given by:

Table 1. Some of the hydrodynamic parameters used in the hydrodynamic model. For a detailed description of the parameterization cf. Sandulescu et al. (2006)

r	25	km	island radius
u_0	0.18	$\frac{\mathrm{m}}{\mathrm{s}}$	horizontal main flow velocity
u_E	0.02	$\frac{\mathrm{m}}{\mathrm{s}}$	velocity of the Ekman flow
ω	55×10^3	$\frac{\mathrm{m}^2}{\mathrm{s}}$	vortex strength

$$\begin{aligned}
\frac{d}{dt}N &= S(N_0-N) - \sum_{i=1}^{2}\beta_i \frac{N}{k_i+N}P_i + \mathrm{rec} \\
\frac{d}{dt}P_i &= \beta_i \frac{N}{k_i+N}P_i - \frac{\alpha\eta P_i^2}{\alpha+\eta P_i^2}Z - \mu_{P_i}P_i \ , \ i\in\{1,2\} \\
\frac{d}{dt}Z &= \gamma\sum_{i=1}^{2}\frac{\alpha\eta P_i^2}{\alpha+\eta P_i^2}Z - \mu_Z Z^2 \\
\mathrm{rec} &= \mu_N[\sum_{i=1}^{2}((1-\gamma)\frac{\alpha\eta P_i^2}{\alpha+\eta P_i^2}Z + \mu_{P_i}P_i) + \mu_Z Z^2] \ .
\end{aligned} \tag{2}$$

The first term in the equation of nutrients N describes the vertical mixing of nutrients from deep ocean water into the mixed layer and leads to an exponential relaxation with the rate S to a nutrient concentration N_0 below the thermocline. The nutrient consumption by phytoplankton is given by a Holling type II functional response which is based on the assumption of a randomly searching organism while the grazing by zooplankton is given by a Holling type III response based on the assumption of reward dependent searching (Gurney and Nisbet, 1998). The factor γ takes into account that not all consumed phytoplankton is converted into biomass. We assume a linear natural mortality for the phytoplankton and a quadratic one for the zooplankton. The latter is chosen to take into account a higher mortality caused by grazing of other top predators which are not included in

Table 2. Ecological parameters used in the biological model Eq. (3) (not characterizing the functional groups of phytoplankton).

N_0	8.0	$\frac{\text{mmolN}}{\text{m}^3}$	nutrient concentration in deep ocean
μ_N	0.2		regeneration efficiency
γ	0.75		assimilation efficiency
α	2	d^{-1}	maximum grazing rate
μ_Z	0.2	$\left(\text{d}\frac{\text{mmolN}}{\text{m}^3}\right)^{-1}$	zooplankton mortality
η	1.0	$\left(\text{d}\left(\frac{\text{mmolN}}{\text{m}^3}\right)^2\right)^{-1}$	prey capture rate

Table 3. Ecological parameters characterizing the two functional groups of phytoplankton.

	P_1	P_2		
β_i	3	1	d^{-1}	maximum growth rate
k_i	2	0.25	$\frac{\text{mmolN}}{\text{m}^3}$	half saturation constant
μ_{P_i}	0.15	0.05	d^{-1}	phytoplankton mortality

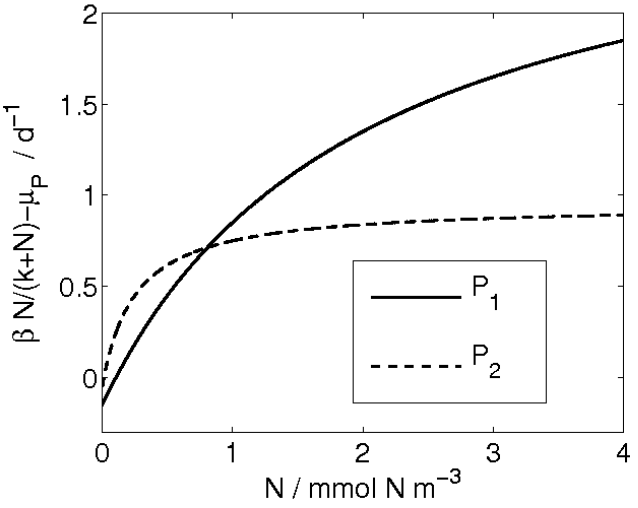

Fig. 2. Effective growth rate (growth minus mortality neglecting the grazing by zooplankton) of the two different phytoplankton groups dependent on available nutrients. Intersection at $N = 0.81\ \frac{\text{mmolN}}{\text{m}^3}$.

this model. Furthermore, a part μ_N of all organic matter is degraded by bacteria leading to an additional nutrient input modeled as a recycling term (rec) in the nutrient equation.

The parameters not characterizing the different phytoplankton groups are chosen as in Pasquero et al. (2005) (Table 2).

The two different phytoplankton groups are grazed by the zooplankton with the same preference. They differ only in their mortality, their maximum growth rate and half saturation constants. We choose these parameters (Table 3) based on a detailed analysis of Edwards (1997) about the ranges of ecological parameters.

Phytoplankton group P_1 has a higher maximum growth rate ($\beta_1 > \beta_2$), while phytoplankton group P_2 has a lower half saturation constant ($k_1 > k_2$). Furthermore, P_1 has a higher mortality $\mu_{P_1} > \mu_{P_2}$.

2.2.1 The dynamics of the food web without hydrodynamics

The dominating species in the model is the one with the higher effective growth rate $\beta\frac{N}{k+N} - \mu_P$ (Fig. 2). For a low nutrient availability species P_2 performs better due to its lower half saturation constant. For higher values of N however, species P_1 grows faster caused by its higher maximum growth rate. This effect is enhanced by our choice of mortalities.

The nutrient availability N strongly depends on the upwelling rate S. Thus, a high S leads to the dominance of species P_1 due to higher nutrient availability and vice versa (Fig. 3). For $S < S_c \approx 0.013\ \frac{1}{d}$ phytoplankton group P_1 does not exist at all corresponding to competitive exclusion of this group. Beyond a transcritical bifurcation at S_c, P_1 and P_2 can coexist with a dominance of P_2 over P_1 for $S < 0.1035\frac{1}{d}$ and P_1 over P_2 for $S > 0.1035\frac{1}{d}$. For a further increasing S the growth rate of phytoplankton converges to the maximum growth rate. Both P_1 and P_2 remain constant under a further change of S (Fig. 3).

The coexistence of the two species on one nutrient is possible due to the presence of a predator in the model. The consumption of the phytoplankton groups depends on their concentration and is therefore equivalent to a density-dependent mortality which allows for coexistence of more species than resources in an ecological model (Gurney and Nisbet, 1998; Gross et al., 2009).

For the interplay of biological growth and hydrodynamics not only the long term behavior but also the transient behavior of the model is important. In the case of a low upwelling rate ($S_{\text{low}} = 0.00648\ \frac{1}{d}$) and low initial concentrations, P_2 shows a peak before converging to the stationary state (upper panel of Fig. 4). The same behavior can be observed for P_1 in the case of high upwelling $S_{\text{high}} = 0.648\ \frac{1}{d}$ (Fig. 4 lower panel). We will refer to this temporal evolution as a bloom-like behavior in the following.

2.3 Coupled model: reaction-advection-diffusion equations

Coupling the biological model to the hydrodynamic motion yields the following set of reaction-advection-diffusion equations:

$$\partial_t c = -\boldsymbol{u} \bigtriangledown c + F_c + D \bigtriangleup c\ ,\ c \in \{N, P_1, P_2, Z\} \tag{3}$$

with the Eulerian field quantity $c = c(\boldsymbol{r}, t)$, the velocity field $\boldsymbol{u} = (u, v)$ from Eq. (1) and the biological terms F_c from Eq. (3). The diffusion term takes the small scale turbulence

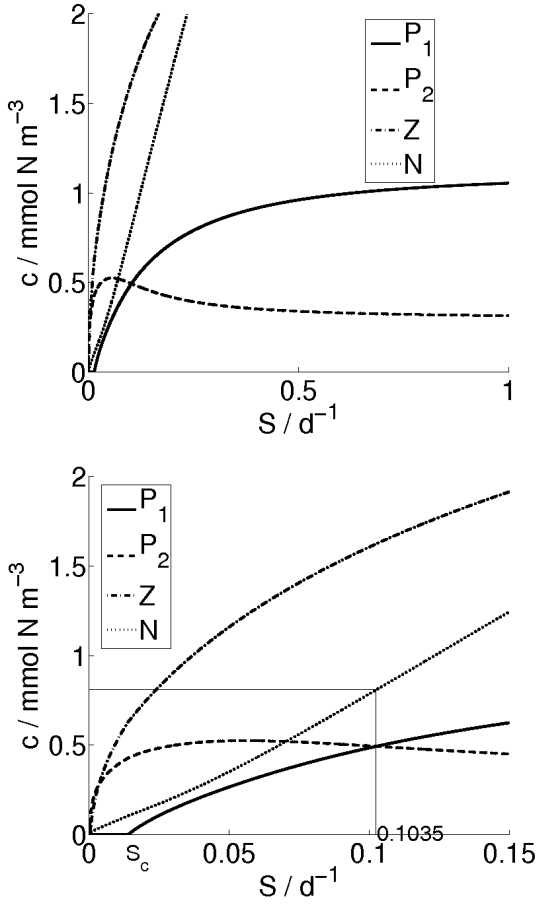

Fig. 3. Stationary solutions of the biological model dependent on the upwelling rate S. For $N = 0.81\ \frac{\text{mmolN}}{\text{m}^3}$, $S = 0.1035\ \frac{1}{d}$ species P_1 becomes the dominant species. The lower panel is a closeup of the upper panel.

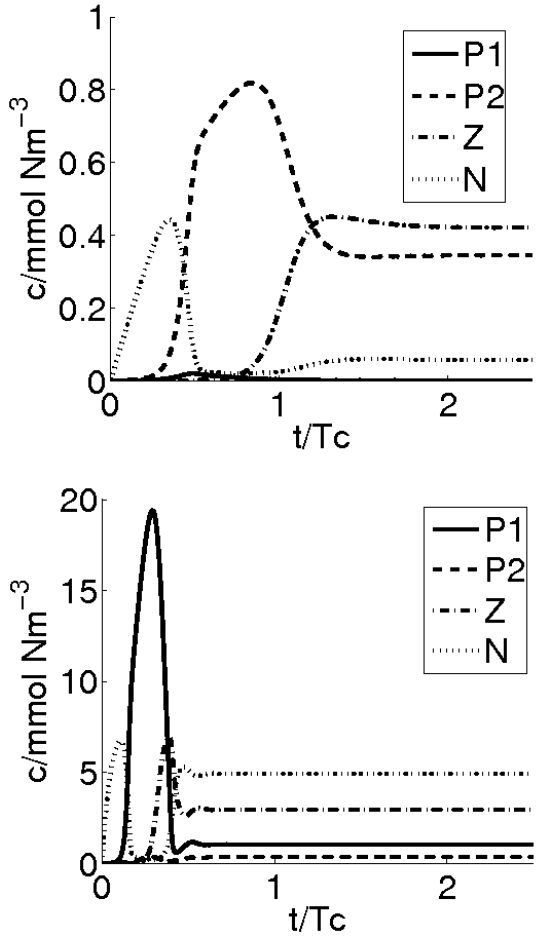

Fig. 4. Time evolution of the biological model with $S = 0.00648\,\text{d}^{-1}$ (upper panel) and $S = 0.648\,\text{d}^{-1}$ (lower panel). The initial concentrations are given by: $c = 10^{-3}\,\text{mmol N m}^{-3}$, $c \in \{N, P_1, P_2, Z\}$.

into account which cannot be resolved by our large scale stream function. We use $D = 10\ \frac{\text{m}^2}{\text{s}}$ as the Okubo estimation of eddy diffusivity at scales of about 10 km (Okubo, 1971), which corresponds to the scales of the mesoscale structures in the flow.

To model the upwelling region (Fig. 1) we vary the upwelling rate S in space ($S = S(\boldsymbol{r}, t)$). Outside the upwelling region we choose $S = S_{\text{low}} = 0.00648\ \frac{1}{d}$, which lies in a range suggested by Edwards (1997). Within the upwelling region we set $S = S_{\text{high}} = 0.648\ \frac{1}{\text{d}}$ to model a strong, e.g. a hundred times larger, vertical transport of nutrients. For the low value $S_{\text{low}} = 0.00648\frac{1}{\text{d}}$ the purely biological model leads to the stationary state $P_1 = 0.0\,\text{mmol N m}^{-3}$, $P_2 \approx 0.82\,\text{mmol N m}^{-3}$, $Z = 0.43\,\text{mmol N m}^{-3}$, $N = 0.65\,\text{mmol N m}^{-3}$ (see also Fig. 4). Thus, species P_1 does not survive and therefore would not occur in the observation region without the additional local upwelling zone.

Additionally, we need to specify the concentrations of nutrients and plankton entering the observation region with the main flow (left boundary in Fig. 1). Here, we assume that the open ocean is oligotrophic containing nutrients and plankton at very low concentrations. We assume these concentrations to be even lower than the steady state of the biological model in the observation area. This assumption is justified since in shallower regions around an island concentrations of nutrients and plankton are likely to be higher than in the open ocean due to additional nutrient input from the resuspension of sediment. Therefore, we choose for this study an inflow of very low concentrations ($c = 10^{-3}\ \text{mmolN m}^{-3}$, $c \in \{N, P_1, P_2, Z\}$). We did not choose an equilibrium solution of the model as inflow since in this case species P_1 would not be present and therefore this would lead to a one species model as analyzed in Sandulescu et al. (2008). Sandulescu et al. (2008) also discussed the role of the inflow conditions in detail. We believe that it is not unrealistic to allow a low

inflow of both species. There are many effects which enable coexistence and could allow a nonzero value of species P_1 in the inflow. Some of these effects are environmental fluctuations (Lai and Liu, 2005) and intermediate disturbances (Shea et al., 2004). Furthermore, in systems with more than one nutrient intrinsic chaotic fluctuations can even lead to more surviving species than types of nutrients (Huisman and Weissing, 1999). Despite that we do assume that in the observation region the investigated effects are more important than the underlying complex behavior and are thus well enough described by our simplified model. The choice of $c = 10^{-3}$ may also seem arbitrary but choosing different kinds of low inflow conditions (e.g. randomly chosen), even setting P_1 two magnitudes lower than P_2 did not change our results qualitatively.

The system (3) is solved by means of a semi-Lagrangian algorithm. A discussion of semi-Lagrangian methods can be found in Strain (1999, 2000).

3 Results

In this section we first present the simulation results from the coupled model described in Sect. 2.3. Since we are interested in the influence of the mesoscale hydrodynamic structures on the competition of the two different phytoplankton groups we first focus on their spatio-temporal distribution. It turns out that for our model the inhomogeneous nutrient input due to local upwelling and the hydrodynamic motion allow a separation of the phytoplankton groups into different regions of the flow. We study the mechanism leading to these patterns of dominance and show that the two key factors of this mechanism are the hydrodynamic transport and the interplay of hydrodynamic and biological time scales. We also reveal that the transport phenomena do not exclusively occur for our rather arbitrary choice of upwelling region and vortex strength ω. Furthermore, we investigate the influence of the eddy diffusivity D and the vortex strength ω on the average abundances of the phytoplankton groups in the entire observation area.

3.1 Spatio-temporal distribution of the phytoplankton groups

To investigate the interplay of the hydrodynamic motion and the competition between the two phytoplankton groups we first analyze the spatio temporal distribution of the two groups. Our first observation is that these distributions are strongly inhomogeneous and do no relate to the position of the upwelling region in a simple way. Furthermore, the inhomogeneous nutrient input and the mesoscale hydrodynamic motion seem to allow a separation of the two phytoplankton groups into different regions of the observation area.

A high abundance of the phytoplankton group P_2 can be observed in the center of every vortex and around the island (Fig. 5c, d). The whole temporal behavior revealed that group P_2 shows a localized plankton bloom *in every vortex* as observed in the one species model by Sandulescu et al. (2008, 2007). In the lower vortex an even higher abundance of group P_2 can be found particularly in the edge of the vortex (compare c and d in Fig. 5). Contrary to P_2, the group P_1 does not occur in the upper vortex, but only in the edge of *every second vortex*, namely the lower one, not entering its center. This is somehow counterintuitive since P_1 needs more nutrients which are released in the upwelling region closer to the upper vortex. Furthermore, a high abundance can be observed in a filament in the upper right area of the observation region. In these rather small regions P_1 shows a bloom-like behavior with an even higher abundance than group P_2 (Fig. 5c, d).

Let us now study more precisely the abundance of phytoplankton in the different regions of the vortices. To this end, we use the Okubo-Weiss parameter W (Okubo, 1970; Weiss, 1991) to characterize the different regions of the vortex. The Okubo-Weiss parameter is defined by:

$$\underset{\text{(normal strain)}^2}{W = (\partial_x u - \partial_y v)^2} \underset{\text{(shear strain)}^2}{+(\partial_x v + \partial_y u)^2} \underset{\text{(vorticity)}^2}{+(\partial_x v - \partial_y u)^2} \quad (4)$$

We define the *interior of the vortex* by $W < -10^8 \frac{1}{d^2}$ describing the region dominated by vorticity. By contrast, we denote the region with a very high strain $W > 10^8 \frac{1}{d^2}$ as the *exterior of the vortex* and the union of both regions as the complete vortex. The choice of these numbers, leaving out the region $-10^8 \frac{1}{d^2} < W < 10^8 \frac{1}{d^2}$, lead to a good identification of the vortex structures (Fig. 6).

Looking at the average abundances in these defined regions again reveals the different periodicity of the blooms of the different phytoplankton groups in the vortices (Fig. 7). Phytoplankton group P_2 shows a peak every $0.5\ T_c = 15$ d corresponding to the occurrence of two vortices in the period of the flow ($1\ T_c = 30$ d). By contrast, the group P_1 shows a peak every $1\ T_c = 30$ d only, since it occurs only in every lower vortex.

A high abundance of P_2 can be found in the exterior as well as the interior of the vortex while group P_1 is only occurring in the exterior of the vortex (Fig. 8).

Hence, we find that the mesoscale hydrodynamic motion seems to allow an inhomogeneous distribution of dominance patterns. The composition of the phytoplankton community is different for the two different vortices. The phytoplankton group better adapted to a high nutrient availability only occurs in every lower vortex. Furthermore, it just occurs in a small ring in the exterior of the vortex. Therefore, the question arises which mechanism is responsible for the distinctly different spatio-temporal distributions of the competing plankton groups.

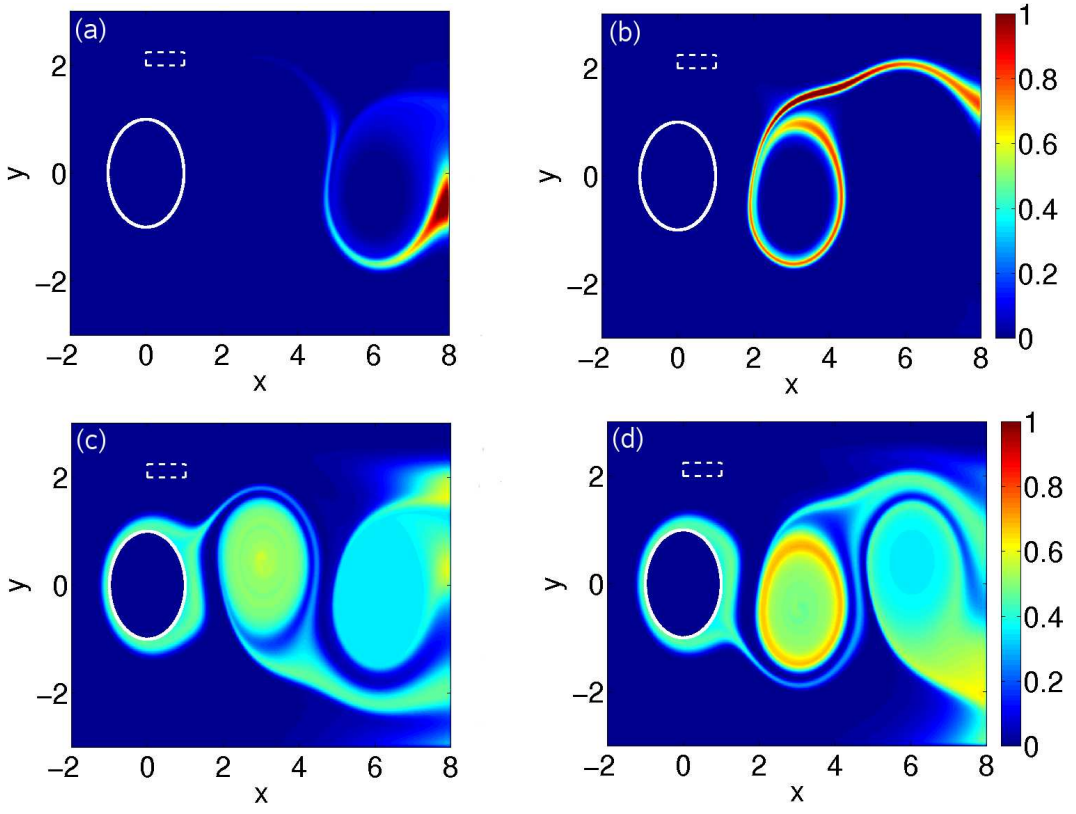

Fig. 5. Colors denote the abundance of phytoplankton group (in $\frac{\text{mmolN}}{\text{m}^3}$). **(a)** P_1 at $t = 5.34\ T_c$, **(b)** P_1 at $t = 5.84\ T_c$, **(c)** P_2 at $t = 5.34\ T_c$, **(d)** P_2 at $t = 5.84\ T_c$. Dashed white rectangle: upwelling region. white circle: island. Spatial coordinates are given in units of 25 km.

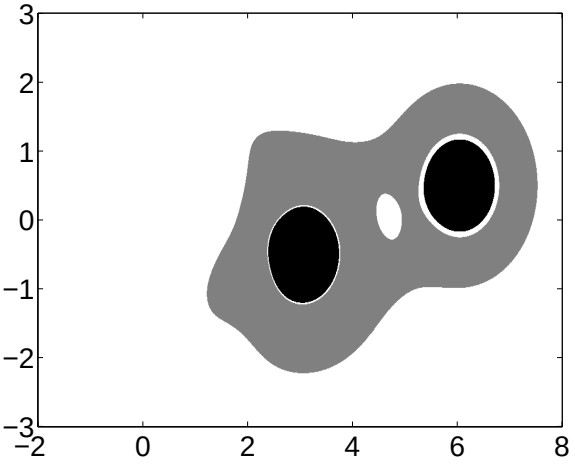

Fig. 6. Okubo-Weiss Parameter W at $t = 0.86\ T_c$. Dark Grey: Exterior of the vortices ($W > 10^8 \frac{1}{d^2}$, very high strain). Black: Interior of the vortices ($W < -10^8 \frac{1}{d^2}$, very high vorticity).

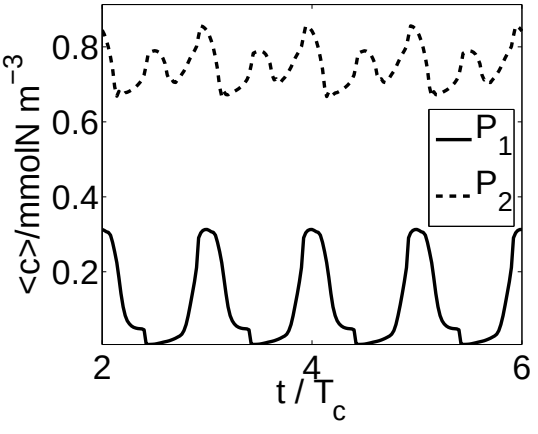

Fig. 7. Spatially averaged abundance of the phytoplankton groups in the complete region of vortices (exterior and interior). Note the different periodicity of the two phytoplankton groups.

3.2 The mechanism leading to the inhomogeneous dominance patterns

In this subsection we will study the mechanism leading to the patterns described above. Furthermore, we will show that the observed structures are not only occurring for our special set of chosen hydrodynamic parameters. Particularly, the position of the upwelling region will be discussed. It turns out that the main features of the spatio-temporal distribution, can be understood by considering the limit case of vanishing

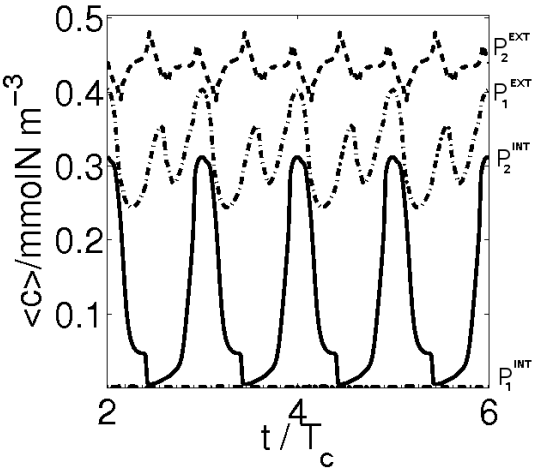

Fig. 8. Spatially averaged abundance of the phytoplankton groups in the region of vortices. P_1^{EXT}: P_1 in the exterior of the vortices. P_1^{INT}: P_1 in the interior of the vortex. P_2^{EXT}: P_2 in the exterior of the vortices. Dashed-dotted line: P_2^{INT} in the interior of the vortices.

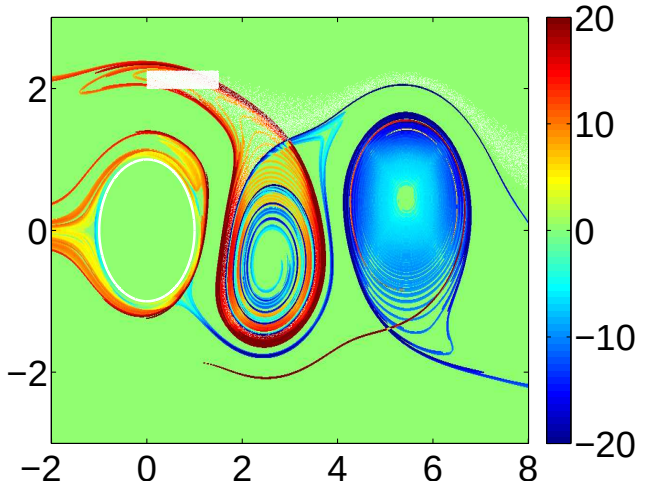

Fig. 10. Finite Size Lyapunov-exponents (plotted as $\lambda_+(\boldsymbol{r},t) - \lambda_-(\boldsymbol{r},t)$). Negative values: Unstable Manifolds. Positive Values: stable Manifolds. White dots: Tracers released in the upwelling region.

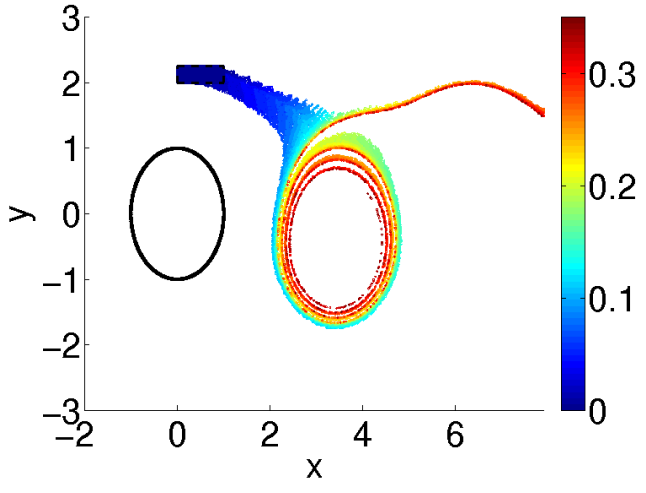

Fig. 9. Tracers released in the upwelling region $[0,1]\times[2,2.25]$ at $t = 5.84\ T_c$. The colors denote the time they have been in the observation region (backward residence time).

diffusion ($D \to 0$). Thus, advection plays the major role for the formation of the observed patterns and the dynamics can be easily described from a Lagrangian point of view. This way, we can conclude that the observed patterns are mainly caused by the advective transport and the interplay of biological and hydrodynamic time scales.

3.2.1 Hydrodynamic transport

The upwelling region obviously plays an important role for the observed mesoscale structures of plankton concentrations. Parcels crossing this region contain a lot of nutrients essential for the growth of phytoplankton. To get some insight in the transport of these parcels we follow two ideas: First, we study the transport of parcels crossing the upwelling region by simply putting tracers in the upwelling region and follow their trajectories. This reveals the importance of the transport for the observed dominance patterns. Second, we will discuss the transport from a more general point of view. The consideration of finite-size Lyapunov-exponents (FSLE) and residence times in the observation region will allow us to comment on the robustness of the observed transport phenomena. The influence of hydrodynamic parameters and the position of the upwelling region will be discussed. The interplay of the hydrodynamic transport and the biological processes will be investigated in the subsequent subsection.

Transport of tracers starting in the upwelling region

Tracers released in the upwelling region get entrained by every lower vortex only. They spiral inwards (Fig. 9) but do not reach the center of the vortex before the vortex disappears due to dissipation. Hence, the tracers leave a big circular region out in their path.

Comparing these transport structures with the distribution of group P_1 (Fig. 5b) indicates that this kind of transport plays a major role for the dominance of phytoplankton P_1 in the ring in the exterior of the lower vortex. Since phytoplankton group P_1 does not reach a high abundance in the case of a weak upwelling (Sect. 2.2.1) it can only grow in parcels having crossed the upwelling region. Therefore, the union of all trajectories of these fluid parcels is the spatio-temporal set where a strong growth of P_1 is possible. This explains the similarities in the tracer distribution of Fig. 9 and the distribution of P_1 in of Fig. 5b.

Dependence on the position of the upwelling region

Since the described transport phenomena play an important role for the observed phenomena it is crucial to show that this kind of transport does not only occur exclusively for our special choice of upwelling region and on other hydrodynamic parameters such as the vortex strength. We investigate the two main effects, (i) that tracers get entrained by every lower vortex only and (ii) that they do not enter its interior.

Looking at possible transport barriers in the flow allows us to study transports independently from initial tracer positions. We investigate these transport barriers by calculating finite size Lyapunov-exponents (FSLE) of the flow (Aurell et al., 1997), a method which has been successfully applied to geophysical flows in d'Ovidio et al. (2004); Rossi et al. (2008); d'Ovidio et al. (2009). The FSLE are a measure for the exponential divergence (and convergence, respectively) of the trajectories of initially nearby tracers. We obtain one Lyapunov-exponent $\lambda_+(\boldsymbol{r},t)$ for the flow integrated forward in time and a different one ($\lambda_-(\boldsymbol{r},t)$) for the flow integrated backwards in time. Maxima in the spatial distribution of λ_+ approximate stable manifolds of the chaotic flow while maxima of λ_- approximate unstable manifolds (Aurell et al., 1997). The stable and unstable manifolds are transport barriers of the flow and cannot be crossed by tracers.

The calculated FSLE nicely show the mesoscale structures of manifolds corresponding to the two vortices in the flow field (Fig. 10). Tracers released in the upwelling region can only get entrained by the vortices if the transport barriers allow a way of entrainment. Throughout this paper entrainment means that tracers will enter the vortex and spiral inwards along the unstable manifolds of the chaotic saddle (cf. 2.1) as observed in (Fig. 10). However, looking at this snapshot of manifolds can be misleading. Due to the non-stationarity of the flow the manifolds are moving and tracers that seem to be trapped in a snapshot actually follow unexpected trajectories. Analyzing the complete time series of Lyapunov-exponents leads to the conclusion that tracers once entrained by a vortex cannot leave the vortex anymore. The vortices in our flow move approximately three times slower than the main stream outside the vortices. Thus, tracers entrained by the vortices remain longer in the observation region than others.

This can be visualized by plotting the forward residence time $\tau^+_{\mathrm{res}}(\boldsymbol{r},t)$ of tracers in the flow, which is the time tracers will remain in the observation region when starting from $\boldsymbol{r}$ at time t. A high τ^+_{res} obviously indicates that tracers are or will be entrained by a vortex. Investigating the time series of τ^+_{res} we can identify regions from where tracers are or will be entrained by a vortex. At time $t = 0.36\ T_c$ (Fig. 11a) the yellow-green area shows the region from which tracers will be entrained by the lower vortex. This *area of entrainment* is visible even though the vortex itself, in terms of high vorticity and unstable manifolds in the center, has not evolved yet. Looking at further snapshots of $\tau^+_{\mathrm{res}}(\boldsymbol{r},t)$ reveals the temporal evolution of the *area of entrainment* of the lower vortex (yellow-green area in Fig. 11a, green area in panel b, light blue area in panel c). The green region Fig. 11d shows the area of entrainment for the upper vortex.

Tracers crossing the upwelling region can only get entrained by the vortex if there is an overlap between the area of entrainment of the vortex and the upwelling region as seen in Fig. 11c. Everywhere the area of entrainment passes an upwelling region would lead to entrainment of tracers. The area of entrainment of the upper vortex however does not depart far from the island (Fig. 11d) and thus tracers can only be entrained by the upper vortex if the upwelling region is very close to the island. This yields the existence of a whole spatial area of possible upwelling regions where tracers get entrained by the lower vortex only. Therefore, the phenomenon of entrainment of nutrients by every lower vortex only does not exclusively occur for our special choice of the upwelling region. However, if the upwelling region is too far away from the island the entrainment by any of the vortices does not occur at all since none of these areas of entrainment ever touch the upwelling region.

We have shown that the phenomenon of entrainment by the lower vortex only does not exclusively occur for our rather arbitrary choice of upwelling region. This still leaves the question if tracers entrained by the lower vortex can enter its interior for a different position of the upwelling region or different hydrodynamic parameters. Releasing tracers at the left boundary of the observation region shows that only tracers flowing into the observation region at $y < 0$ can enter the interior of the lower vortex (Fig. 12 upper panel) which proved to be true for every set of realistic hydrodynamic parameters. Therefore, an upwelling region at $y > 0$ does not allow tracers to enter the interior of the lower vortex. This seems to be a rather robust result. As a consequence the fluid parcels crossing the upwelling region and hence developing a bloom of P_1 are only found in the exterior of the lower vortex.

Dependence on the vortex strength ω

The position, form and size of the area of entrainment of the vortices is determined by the set of hydrodynamic parameters. This can lead to critical values of hydrodynamic parameters. A very important parameter is the vortex strength ω which strongly influences the strength of mixing in the wake of an island. A smaller vortex strength leads to a smaller area of entrainment of the vortices and thus to a smaller overlap with the upwelling region (compare Fig. 11c and Fig. 13). This leads to a critical value of the vortex strength, which has to be crossed in parameter space so that entrainment by a vortex is possible.

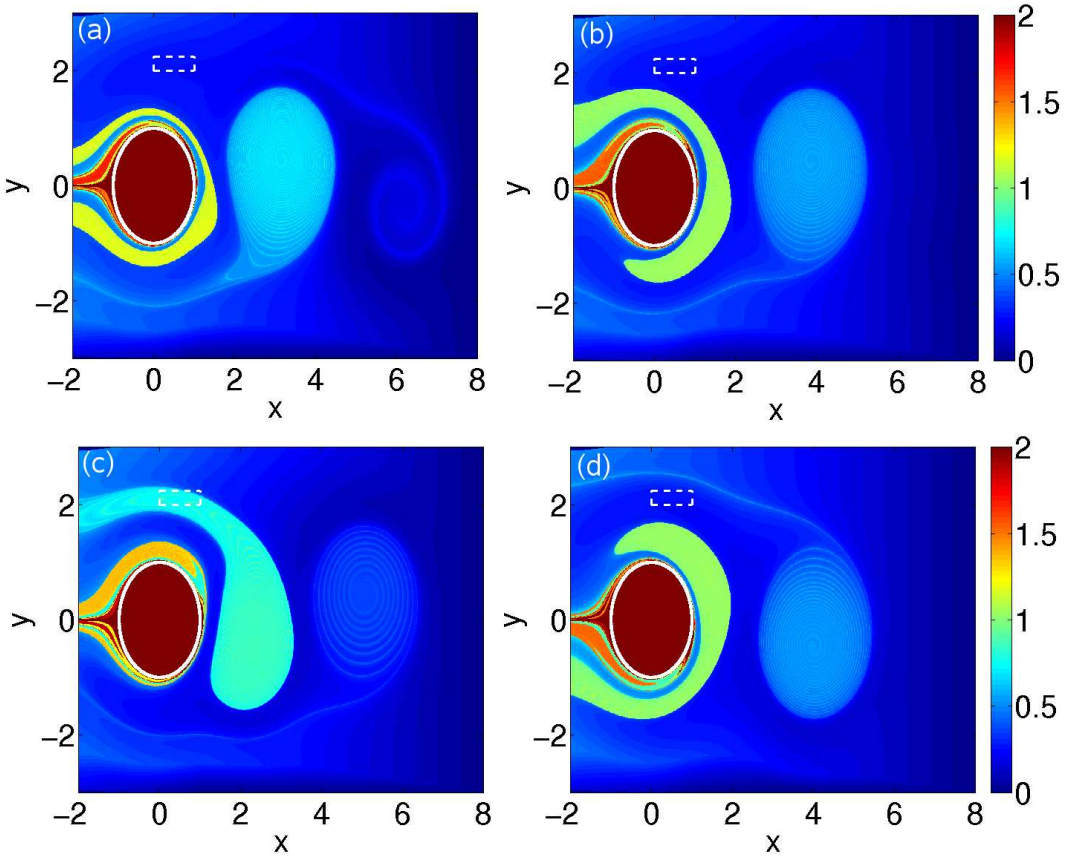

Fig. 11. Colors denote the forward residence times $\frac{\tau^{+}_{\mathrm{res}}(\boldsymbol{r},t)}{T_c}$ at $t = 0.36\ T_c$ **(a)**, $t = 0.48\ T_c$ **(b)**, $t = 0.68\ T_c$ **(c)**, $t = 1.00\ T_c$ **(d)**. The yellow-green region ($\frac{\tau^{+}_{\mathrm{res}}(\boldsymbol{r},t)}{T_c} \approx 1.2$) in **(a)**, the green region ($\frac{\tau^{+}_{\mathrm{res}}(\boldsymbol{r},t)}{T_c} \approx 1$) in **(b)** and the light green region ($\frac{\tau^{+}_{\mathrm{res}}(\boldsymbol{r},t)}{T_c} \approx 0.8$) in **(c)** are the areas of entrainment of the lower vortex. The overlap with the upwelling region **(b)** (dashed white rectangle) allows for entrainment of parcels crossing the upwelling region. The green area ($\frac{\tau^{+}_{\mathrm{res}}(\boldsymbol{r},t)}{T_c} \approx 1$) in **(d)** shows the area of entrainment of the upper vortex. This area does not overlap with the upwelling region (dashed white rectangle) for all times. Thus, entrainment of parcels crossing the upwelling region is not possible for the upper vortex.

Comment on tracers entering the vortex

As already mentioned above, tracers having crossed the upwelling region and having been entrained by the vortex spiral inwards along the unstable manifolds (Fig. 10). Their motion becomes mainly rotational and therefore they do not enter the center of the vortex in the finite lifetime of the vortex. This leads to the question how tracers get into the interior of the vortex at all. The only possible explanation is that they have already been in the area of entrainment before the complicated structures of unstable manifolds evolve. They directly flow into the yellow-green region of Fig. 11c when entering the observation region.

3.2.2 Interaction of hydrodynamic and biological time scales

We have shown that for a certain range of hydrodynamic parameters and of locations of the upwelling region the growth of species P_1 in the edge of every lower vortex is possible due to the transport of nutrient rich water parcels starting in the upwelling region. However, having crossed the upwelling region is only a necessary condition for a high abundance of P_1. The second key factor is the interplay of hydrodynamic and biological time scales. The abundance of both species in a parcel evolves in time and thus depends on (i) the time P_i needs to grow in a parcel, (ii) the time the parcel has been in the observation region $\tau^{-}_{\mathrm{res}}(\boldsymbol{r},t)$ (Fig. 14), (iii) the time the parcel has entered the upwelling region and (iv) the time the parcel has spent there. Thus, we analyze in this section the interplay of the different time scales by analysing the system from a Lagrangian perspective and in the limit of zero diffusion.

In the limit case of zero diffusion ($D \to 0$) Eq. (3) becomes:

$$\partial_t c = -\boldsymbol{u} \bigtriangledown c + F_c(c)\ ,\ c \in \{N, P_1, P_2, Z\} \tag{5}$$

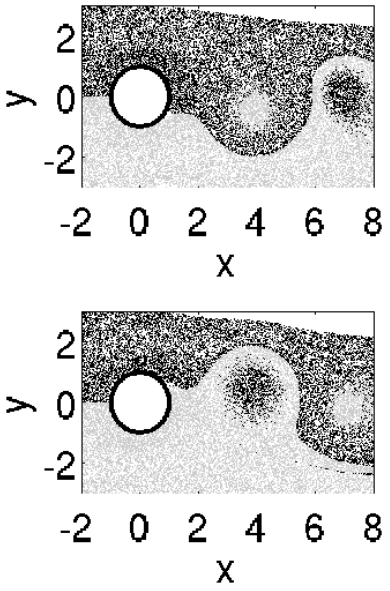

Fig. 12. Tracer released at the left boundary, black dots: tracer released at $y > 0$, grey dots: tracer released at $y < 0$. upper panel: $t = 4.0\ T_c$, lower panel: $t = 4.5\ T_c$.

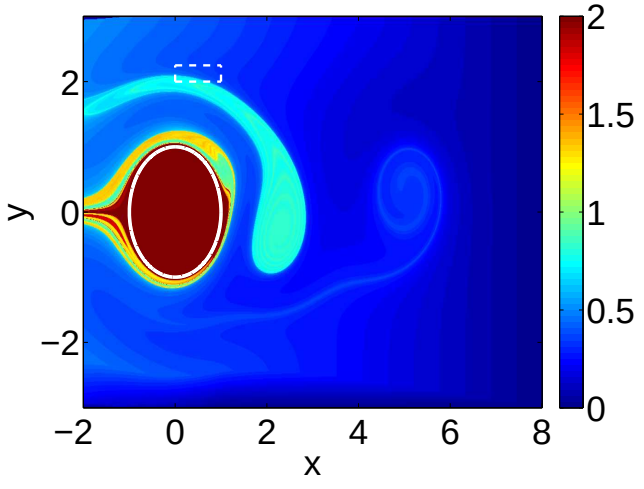

Fig. 13. Colors denote the forward residence times of the flow $\frac{\tau_{\text{res}}^{+}(\boldsymbol{r},t)}{T_c}$ for $\omega = \frac{1}{4}55 \times 10^3 \frac{\text{m}^2}{\text{s}}$. The area of entrainment and the overlap with the upwelling region become smaller (compared to the situation in Fig. 11c with: $\omega = 55 \times 10^3\ \frac{\text{m}^2}{\text{s}}$).

From the Lagrangian point of view the concentration $c_{\text{L}}(t)$ along the trajectory $\boldsymbol{r}_{\text{L}}(t)$ of an infinitesimal fluid parcel is considered, where $\boldsymbol{r}_{\text{L}}$ is a solution of:

$$\dot{\boldsymbol{r}} = \boldsymbol{u},\ \boldsymbol{r}(0) = \boldsymbol{r}_L(0)\ . \tag{6}$$

Then Eq. (5) becomes:

$$\frac{d}{dt} c_{\text{L}} = F_c(c_{\text{L}}(t))\ ,\ c_{\text{L}}(t) = c(\boldsymbol{r}_{\text{L}}(t), t)\ . \tag{7}$$

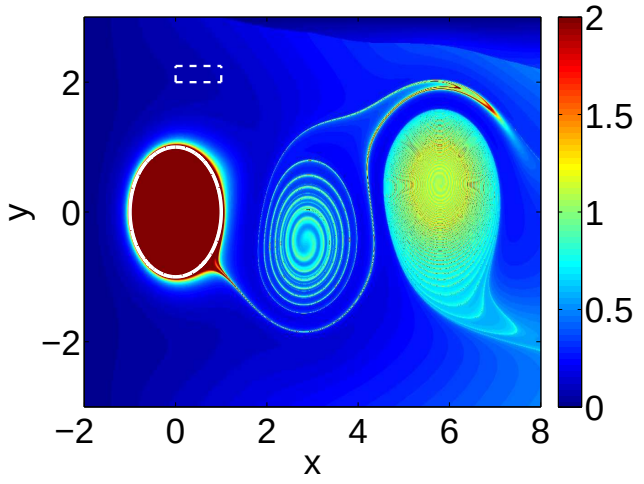

Fig. 14. Colors denote the backward residence times $\frac{\tau_{\text{res}}^{-}(\boldsymbol{r},t)}{T_c}$ of the flow field for $t = 0.8\ T_c$.

This way the dynamics of a reaction-advection system can be understood simply as the dynamics of infinitely many fluid parcels, which evolve following Eq. (7). Since diffusion is assumed to be zero, there is no coupling between the individual parcels and they evolve independently. However, not all fluid parcels evolve identically. Due to the upwelling region in our model the nutrient input into a parcel depends on its trajectory and thus:

$$F_c(c_{\text{L}}(t)) = F_c(c_{\text{L}}(t), S(\boldsymbol{r}_{\text{L}}(t)))\ . \tag{8}$$

However, we can consider two different kinds of parcels: Parcels crossing the upwelling region and parcels not crossing the upwelling region. The biological model within parcels not crossing the upwelling region evolves as in Fig. 4 (upper panel) following:

$$\frac{d}{dt} c_L^{(1)} = F_c(c_L^{(1)}, S_{\text{low}}) \ \text{ with } c_L^{(1)}(0) = c_0 \quad \text{and } c \in \{N, P_1, P_2, Z\} \tag{9}$$

where c_0 is the concentration at the left boundary of the observation region. Thus, the concentration for a given point and time only depends on the (i) time the species need to grow in the parcel and (ii) the time the corresponding parcel has been in the observation region $\tau_{\text{res}}^{-}(\boldsymbol{r},t)$ (backward residence time):

$$c(\boldsymbol{r},t) = c_{\text{L}}^{(1)}(\tau_{\text{res}}^{-}(\boldsymbol{r},t)). \tag{10}$$

where the trajectory corresponding to $c_{\text{L}}^{(1)}$ has not crossed the upwelling region. Therefore, inhomogeneous concentration distributions can simply be caused by inhomogeneous residence times (Fig. 14) which are typical for open chaotic flows. The backward residence times $\tau_{\text{res}}^{-}(\boldsymbol{r},t)$ of the flow (Fig. 14) show filaments with a residence time of about $1T_c = 30$ d in the interior and exterior of the vortex at ($t = 0.8\ T_c$).

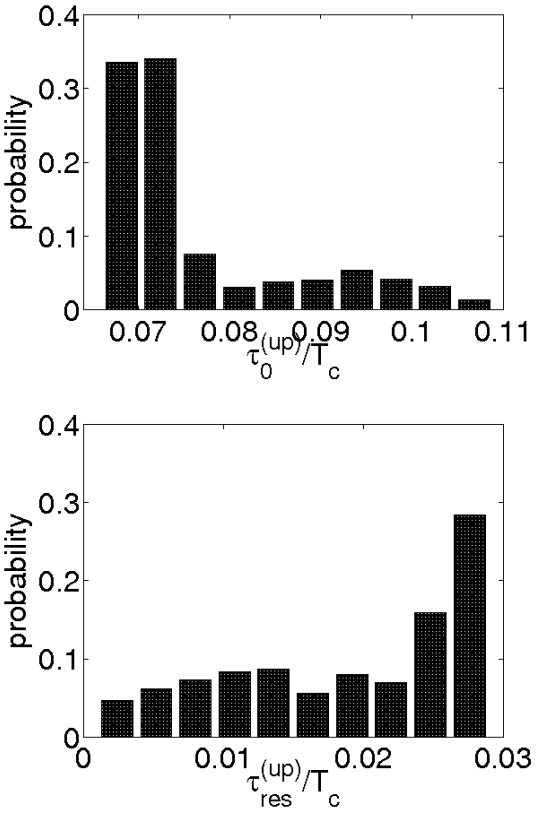

Fig. 15. Histogram of the time τ_0^{up} which particles released at the left boundary of the observation region need to enter the upwelling region (upper panel). Histogram of the residence times $\tau_{\text{res}}^{\text{up}}$ in the upwelling region (lower panel).

The biological time scale of a parcel not crossing the upwelling region is given by the time that group P_2 needs to reach the maximum abundance which is given by $\tau_{P_2} \approx 20\,\text{d}$ (Fig. 4). This allows for high abundance of P_2 in the interior and exterior of the vortex in Fig. 5c and d. The fine structures however are not visible due to strong diffusion in our coupled model (compare Figs. 5d and 14). This described mechanism leads to the bloom-like behavior of species P_2 in both vortices and has also been discussed for the one-species case in Sandulescu et al. (2007, 2008). The plankton inside the vortices has enough time to grow while parcels not being entrained leave the region in around $0.5\ T_c = 15\,\text{d}$ not reaching very high concentrations of P_2.

The second kind of parcels do cross the upwelling region. The biological evolution of these parcels additionally depends on (iii) the time it takes to enter the upwelling region after being released at a boundary and on (iv) the time they spend in the upwelling region. Most parcels enter the upwelling region after $\tau_0^{\text{up}} \approx 0.07\ T_c = 0.75\,\text{d}$ (Fig. 15 upper panel) and leave it again after $\tau_{\text{res}}^{\text{up}} \approx 0.025\ T_c = 0.75\,\text{d}$ (Fig. 15 lower panel). Thus, the majority of these parcels experience a high nutrient input in the time interval $[\tau_0^{\text{up}}, \tau_0^{\text{up}} + \tau_{\text{res}}^{\text{up}}]$ following:

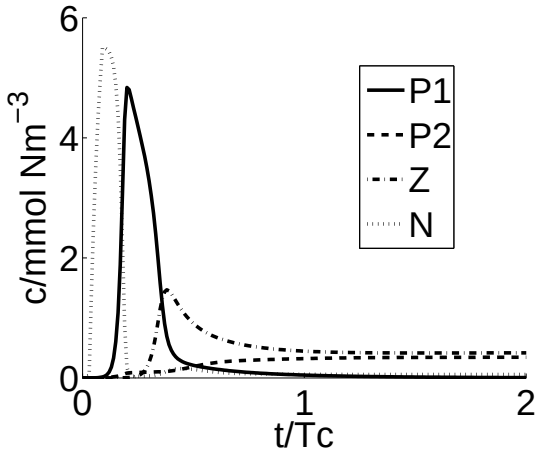

Fig. 16. Biological evolution of a fluid parcel crossing the upwelling region in the time $[0.06, 0.06+0.025]\ T_c$.

$$\frac{d}{dt}c_{\text{L}}^{(2)} = \begin{cases} F_c(c_{\text{L}}^{(2)}, S_{\text{high}}) & , t \in [\tau_0, \tau_0 + \tau_{\text{res}}^{\text{up}}] \\ F_c(c_L^{(2)}, S_{\text{low}}) & , \text{otherwise} \end{cases} \quad \text{with } c_L^{(2)}(t=0) = c_0 \tag{11}$$

This leads to a biological time scale of $\tau_{P_1} \approx 8\,\text{d}$ to reach the maximum abundance (Fig. 16).

In the edge of the lower vortex and in the filament in the upper right area of the observation region tracers with a residence time of about $0.25\ T_c \approx 8\,\text{d}$ can be found (Fig. 9) which matches the biological time scale τ_{P_1} leading to the high abundance of phytoplankton group P_1.

Varying the size and position in a moderate way meaning tracers crossing the upwelling region can still be entrained by the vortex (see Sect. 3.2.1) changes the time scales τ_0^{up} and $\tau_{\text{res}}^{\text{up}}$ which leads to a change of τ_{P_1}.

It turns out that a change in position and therefore τ_0^{up} has only weak effects. It just leads to a small time shift of the biological behavior. The size of the region however has a stronger effect. As an illustrative case we consider a large upwelling region $[0,2] \times [2,3]$ leading to $\tau_{\text{res}}^{\text{up}}$ up to 0.1. Using this value in Eq. (12) yields a much higher peak in the evolution of species P_1. Obviously this will lead to a stronger bloom of P_1 in the spatio-temporal patterns as well. The time scale of the growth of P_1 is only slightly effected with $\tau_{P_1} \approx 0.23\ T_c \approx 7\,\text{d}$. Looking again at Fig. 9 shows that parcels have less time to spiral inwards into the vortex interior but the qualitative behavior will be very similar. We thus conclude that size and position of the upwelling region are of minor importance.

Further simulations varying the vortex strength and the Ekman velocity show no qualitative change in the observed patterns. However, if the vortex strength is too low for any entrainment of nutrients by the lower vortex, the bloom of phytoplankton group P_1 can only be observed in the nutrient plume in the upper right area of the observation region where tracers are horizontally advected without being entrained.

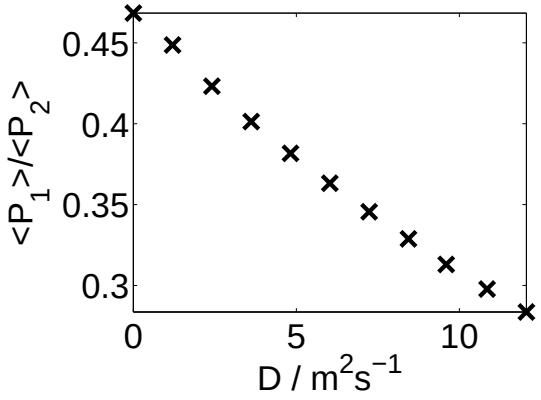

Fig. 17. Ratio of the spatio-temporal average abundance of the two phytoplankton groups versus the eddy diffusivity.

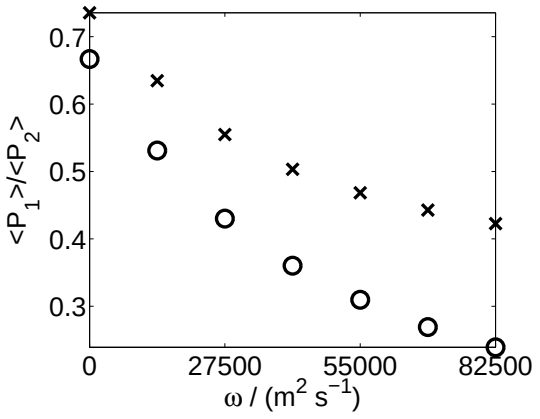

Fig. 18. Ratio of the spatio-temporal average abundance of the two phytoplankton groups versus the vortex strength. circles: $D = 10\frac{\mathrm{m}^2}{\mathrm{s}}$, crosses: $D = 0\frac{\mathrm{m}^2}{\mathrm{s}}$.

3.3 The dependence of average concentrations on diffusivity and vortex strength

In this subsection we will discuss the influence of diffusivity and vortex strength on the spatio-temporal average of the phytoplankton groups. By spatio-temporal average we mean the spatial average over the observation region and the temporal average over one period of the flow. In the previous subsection we tried to explain the phenomenon of inhomogeneous distributions of different phytoplankton groups in the framework of pure advective transport of fluid parcels containing nutrients. However, in the open ocean turbulent mixing is an important process occurring on smaller scales than the mesoscale structures described by our hydrodynamic model. Therefore, we expect that the global picture will be influenced by turbulent diffusion.

For our simulations we chose an eddy diffusivity of $D = 10\ \frac{\mathrm{m}^2}{\mathrm{s}}$. This diffusivity corresponds to a scale of 10 km (Okubo, 1971), the order of mesoscale structures of the flow. Thus, it is an approximate upper boundary but smaller values for D down to $D = 1\ \frac{\mathrm{m}^2}{\mathrm{s}}$ can be realistic, corresponding to a scale of missing turbulent structures of 1 km.

A variation of the eddy diffusivity D in the interval $[0, 12]\ \frac{\mathrm{m}^2}{\mathrm{s}}$ revealed that the abundance of plankton group P_1 decreases with increasing D while the dominance of the phytoplankton group P_2 increases more and more. This dominance appears even more pronounced when plotting the ratio $\frac{P_1}{P_2}$ (Fig. 17). Chaotic advection by our model flow leads to an incomplete mixing of plankton and nutrients in the observation region. The filamental-like transport of nutrients allows for the inhomogeneous plankton distributions in our model. The decrease of $\frac{P_1}{P_2}$ can be attributed to two effects: first, diffusion leads to mixing on smaller scales and therefore weakens the spatial separation of the plankton groups. This effect leads to a higher competition and therefore to a decreasing ratio $\frac{P_1}{P_2}$. Second, and in our case more importantly the small scale mixing leads to a faster dispersion of high nutrient concentrations which is needed for an accelerated growth of group P_1. This effect is enhanced by the mesoscale structures in our flow. Shortly after crossing the upwelling region the nutrient concentration in a fluid parcel rises rapidly before it drops down due to consumption by phytoplankton. Strong diffusion due to strong nutrient gradients sets in before this drop down. The nutrients rotating in the exterior of the vortex diffuse towards the interior where the group P_2 is highly abundant. Due to this high abundance P_2 consumes the nutrients much faster than group P_1. This effect also explains the high abundance of P_2 in the exterior of the lower vortex (compare (c) and (d) in Fig. 5).

Varying the vortex strength ω in a realistic range (according to Sandulescu et al., 2006) reveals a decrease of P_1 and an increase of P_2 with increasing ω also leading to a decrease of the ratio $\frac{P_1}{P_2}$ (Fig. 18). This dependence on ω can have multiple reasons. A change of ω can change the amount of entrained nutrients in the vortices, the time parcels spent in the upwelling region, the residence time of the flow and the net flux through the observation region. Furthermore, a change of ω leads to a change of the impact of diffusion due to a changing size of the vortices as a lower ω leads to a smaller vortex structure (compare again Figs. 11c and 13). Hence, increasing ω means that the ring in the exterior of the vortex becomes larger and with it the area for the diffusive flux. This leads finally to an enhancement of the diffusive influence with increasing vortex strength yielding a decrease of P_1 while increasing the dominance of P_2. This idea is supported by the increase of the diffusive effect $(\frac{P_1}{P_2}(D = 10\ \frac{\mathrm{m}^2}{\mathrm{s}}) - \frac{P_1}{P_2}(D = 0\ \frac{\mathrm{m}^2}{\mathrm{s}}))$ with increasing ω (Fig. 19).

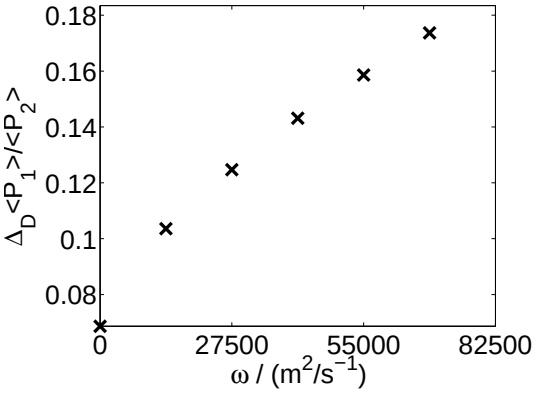

Fig. 19. Diffusive effect $\Delta_D \frac{<P_1>}{<P_2>} := \frac{P_1}{P_2}(D = 10\ \frac{\mathrm{m}^2}{\mathrm{s}}) - \frac{P_1}{P_2}(D = 0\ \frac{\mathrm{m}^2}{\mathrm{s}})$ versus the vortex strength ω.

4 Conclusions

We investigated the spatio-temporal abundance of two different functional groups of phytoplankton competing for the same nutrients in the wake of an island close to an upwelling region. This investigation was carried out by a model of reaction-advection-diffusion equations resulting from the coupling of the hydrodynamic flow in a wake of an island and a simplified biological model of a food web. The biological model consists of three trophic levels: nutrients, two functional groups of phytoplankton and zooplankton. One of the modeled phytoplankton groups can only survive for a high availability of nutrients while the other one was better adapted to a situation of low nutrient availability. The spatio-temporal distribution of these different groups was studied for the situation of a low inflow of nutrients and plankton at the left boundary of the observation region. This low inflow can be understood as an oligotrophic open ocean assumption.

We showed that the interaction of mesoscale vortices and a close enough upwelling region has a strong influence on the composition of the phytoplankton community in the wake of an island. The entrainment of nutrient rich water by the vortices and the interplay of hydrodynamic and biological time scales allow a spatially inhomogeneous distribution of the different phytoplankton groups leading to inhomogeneous dominance patterns. Depending on the transport of nutrients either one or the other phytoplankton group is dominant. It is important to note that the dominance of the group P_1 which prefers high nutrient abundance is not confined to the upwelling region but its bloom-like behavior occurs in other regions far away from the upwelling but connected to it by the fluid flow. Furthermore, we emphasize that P_1 dominates here despite the fact that it would normally die out without the upwelling region.

The composition of the phytoplankton community can be different for vortices differing in position and their sign of vorticity. The group better adapted to a situation of low nutrient availability shows a high abundance around the island itself and *within every vortex*. This localized bloom is caused by the interplay of hydrodynamic and biological time scales. Fluid parcels trapped by the vortices stay long enough in the observation region to experience a bloom-like behavior. This phenomenon has been observed already in Sandulescu et al. (2007, 2008) for only one phytoplankton group. The phytoplankton group which needs a high nutrient availability for survival only occurs in *every second, namely the lower vortex* which is further away from the upwelling region. Additionally, this group can be observed in those places where nutrients are transported with the horizontal main flow. The different signs of vorticity of the vortices lead to different mesoscale structures of transport barriers in the flow. This way nutrients released above the island (not too close) can only get entrained by the lower vortex with a positive vorticity. Therefore, the phytoplankton group needing a high nutrient supply can only survive in the region of the lower vortex. Focusing on the phytoplankton abundances in the vortex regions reveals a different periodicity of abundance peaks for the two phytoplankton groups.

The composition of the phytoplankton community also varies in the interior and exterior region of a vortex. We showed that the fluid parcels coming from the upwelling region and getting entrained by the lower vortex cannot enter the interior of the vortex within its finite lifetime. They spiral inwards but cannot reach the center before the vortex dissipates. This incomplete mixing of the vortices is the first key factor leading to the different composition of the phytoplankton community in the exterior and interior of the vortex. Furthermore, the biological time scale for the growth of the phytoplankton in fluid parcels having crossed the upwelling region plays an important role. The phytoplankton group adapted to a high nutrient availability grows very quickly in these parcels due to a fast uptake of the nutrients which entered the fluid parcel while crossing the upwelling region. Spiralling inwards into a vortex, the nutrients are consumed and the phytoplankton group with high nutrient needs looses the competition with the other phytoplankton group leading to a low abundance in the interior of the vortex. This is a second factor for the rather thin ring of high abundance of this group.

By introducing the concept of an *area of entrainment* of the vortices we showed that the observed transport phenomena and thus also the dominance patterns do not exclusively occur for our special choice of upwelling region and vortex strength. We showed how the vortex strength changes the area of entrainment and how this can lead to the existence of a critical ω not allowing entrainment into any vortex.

Bracco et al. (2000) found similar dominance patterns in the mesoscale vortices of geostrophic turbulence. However, in their work the effect was based on the assumption that the different species enter the observation region from different initial positions. The incomplete mixing of species by eddies protected the less fit species from competition and

hence high abundance of the weaker species could be found in the center of the vortices. This behavior could also be expected in our model if we choose a separated inflow of different phytoplankton groups in the upper and lower part of our left boundary. We also showed that tracers entering the observation region above the island cannot enter the interior of the upper vortex and tracers entering from below the island cannot enter the interior of the lower vortex. This transport phenomenon would also lead to a survival of a less fit phytoplankton group in our model. In contrast to Bracco et al. (2000) we assume a homogeneous inflow condition of plankton and nutrients. Only the inhomogeneous mixing of nutrients due to the mesoscale hydrodynamic structures is of importance for the here reported phenomenon of dominance patterns.

Additionally, our study revealed that the composition of the phytoplankton community depends strongly on the eddy diffusivity of the model. A higher diffusion leads to a more uniform distribution of nutrients and thus to a decrease of the phytoplankton group with high nutrient needs. This effect is even enhanced by an increasing vortex strength of the flow. A higher vortex strength leads to bigger vortices allowing for a bigger area of diffusing nutrients. The interplay of small scale turbulence and hydrodynamic mesoscale structures is therefore an important factor for the composition of the phytoplankton community. In our study we assumed a constant eddy diffusion in the flow. A more realistic approach by estimating spatially varying diffusion coefficients from the velocity field could lead to new insights into this interplay of hydrodynamic motion on different scales and plankton growth.

There are several other factors which might be important but which are not taken into account. One of them is a possible additional upwelling caused by a vortex itself. This upwelling has been studied in e.g. Martin and Richards (2001); Martin and Pondaven (2003). It is hard to parameterize this vertical transport in a two-dimensional model but the effect could definitely be important and should be included into future research. However, this upwelling does not always occur (Paterson et al., 2008).

Another potentially important factor is the dependence of the results on the exact values of the upwelling rates in the deep ocean and in the upwelling region. However, moderate changes of these rates do not lead to a qualitative change of the reported phenomena in our model. The values of the upwelling rates S chosen here yield strongly pronounced patterns providing a good illustration of the effects.

Finally, we discuss the simplicity of our biological model which describes a phytoplankton community as a union of only two functional groups and uses only one kind of nutrient. However, we believe that our main results remain valid when extending the model to various nutrients and more phytoplankton groups. Because of the simplicity of the model we are able to obtain general results. The mechanism of inhomogeneous nutrient transport and the different response of species to nutrient input is likely to play an important role in a realistic ecosystem as well. Of course in this case not only the amount of nutrients is important but also the ratio of different kinds of nutrients. Nevertheless, we expect the same mechanisms to influence strongly the competition among the species and to yield even more complicated dominance patterns of species.

A Kármán vortex street in the wake of an island is an ubiquitous phenomenon in the ocean and we obtained our results for a realistic parameterization guided by the Canary archipelago close to the African Coast. Thus, the flow time scales observed are of a realistic order of magnitude. Since the chosen biological time scales are of a realistic order as well this suggests that similar patterns are likely to occur in reality.

Furthermore, we expect similar mechanisms to be important in various situations since the key ingredients such as inhomogeneous nutrient transport and a different response of species to nutrient concentration or just the ratio of different kinds of nutrients are rather general. Mesoscale hydrodynamic structures inducing inhomogeneous transport of nutrients can be found for example in the general case of two-dimensional mesoscale turbulence. We expect more complex patterns in this case due to the irregular spatial and temporal behavior of the flow. But if the hydrodynamic time scales as e.g. the persistence time of eddies in the flow matches realistic biological time scales the plankton distribution will show a spatio-temporal variability caused by the same mechanism.

Acknowledgements. The authors thank Cristóbal López, Támas Tél and Jens Zahnow for valuable discussions.

Edited by: A. M. Mancho
Reviewed by: three anonymous referees

References

Abraham, E. R.: The generation of plankton patchiness by turbulent stirring, Nature, 391, 577–580, 1998.

Aristegui, J., Tett, P., Hernández-Guerra, A., Basterretxea, G., Montero, M. F., Wild, K., Sangra, P., Hernández-Leon, S., Canton, M., García-Braun, J. A., Pacheco, M., and Barton, E. D.: The influence of island-generated eddies on chlorophyll distribution: A study of mesoscale variation around Gran Canaria, Deep-Sea Res. Part I-Oceanographic Research Papers, 44, 71–&, 1997.

Aurell, E., Boffetta, G., Crisanti, A., Paladin, G., and Vulpiani, A.: Predictability in the large: An extension of the concept of Lyapunov exponent, J. Phys. A-Math. Gen., 30, 1–26, 1997.

Beddington, J. R.: Mutual Interference Between Parasites Or Predators And Its Effect On Searching Efficiency, J. Anim. Ecol., 44, 331–340, 1975.

Benczik, I. J., Toroczkai, Z., and Tél, T.: Advection of finite-size particles in open flows, Phys. Rev. E, 67, 036 303, 2003.

Benczik, I. J., Károlyi, G., Scheuring, I., and Tél, T.: Coexistence of inertial competitors in chaotic flows, Chaos, 16, 043 110, 2006.

Bracco, A., Provenzale, A., and Scheuring, I.: Mesoscale vortices and the paradox of the plankton, P. Roy. Soc. Lond. B-Bio., 267, 1795–1800, 2000.

Bracco, A., Clayton, S., and Pasquero, C.: Horizontal advection, diffusion, and plankton spectra at the sea surface, J. Geophys. Res.-Oceans, 114, C02 001, 2009.

Deangelis, D. L., Goldstein, R. A., and Oneill, R. V.: Model For Trophic Interaction, Ecology, 56, 881–892, 1975.

Denman, K. L. and Gargett, A. E.: Biological Physical Interactions In The Upper Ocean – The Role Of Vertical And Small-Scale Transport Processes, Annu. Rev. Fluid Mech., 27, 225–255, 1995.

d'Ovidio, F., Fernandez, V., Hernández-García, E., and López, C.: Mixing structures in the Mediterranean Sea from finite-size Lyapunov exponents, Geophys. Res. Lett., 31, L17203, doi:10.1029/2004GL020328, 2004.

d'Ovidio, F., Isern-Fontanet, J., López, C., Hernández-García, E., and García-Ladon, E.: Comparison between Eulerian diagnostics and finite-size Lyapunov exponents computed from altimetry in the Algerian basin, Deep-Sea Res. Part I-Oceanographic Research Papers, 56, 15–31, 2009.

Edwards, A. M.: A Rational Dynamical-Systems Approach to Plankton Population Modelling, PhD thesis, University of Leeds, 1997.

Edwards, A. M. and Brindley, J.: Oscillatory behaviour in a three-component plankton population model, Dynam. Stabil. Syst., 11, 347–370, 1996.

Gross, T., Edwards, A. M., and Feudel, U.: The invisible niche: Weakly density-dependent mortality and the coexistence of species, J. Theor. Biol., 258, 148–155, 2009.

Grover, J.: Resource Competition, Springer, The Netherlands, 1997.

Gurney, W. and Nisbet, R.: Ecological Dynamics, Oxford Univ Press United Kingdom, 1998.

Hernández-García, E. and López, C.: Sustained plankton blooms under open chaotic flows, Ecological Complexity, 1, 253–259, 2004.

Huisman, J. and Weissing, F. J.: Biodiversity of plankton by species oscillations and chaos, Nature, 402, 407–410, 1999.

Jung, C., Tél, T., and Ziemniak, E.: Application of scattering chaos to particle transport in a hydrodynamical flow, Chaos: An Interdisciplinary J. Nonlinear Sci., 3, 555–568, doi:10.1063/1.165960, http://link.aip.org/link/?CHA/3/555/1, 1993.

Károlyi, G., Péntek, A., Scheuring, I., Tél, T., and Toroczkai, Z.: Chaotic flow: The physics of species coexistence, P. National. Acad. Sci. USA, 97, 13661–13665, 2000.

Lai, Y. C. and Liu, Y. R.: Noise promotes species diversity in nature, Phys. Rev. Lett., 94, 038102, doi:10.1103/PhysRevLett.94.038102 , 2005.

López, C., Neufeld, Z., Hernández-García, E., and Haynes, P. H.: Chaotic advection of reacting substances: Plankton dynamics on a meandering jet, Phys. Chem. Earth Part B-Hydrology Oceans And Atmosphere, 26, 313–317, 2001.

Maraldi, C., Mongin, M., Coleman, R., and Testut, L.: The influence of lateral mixing on a phytoplankton bloom: Distribution in the Kerguelen Plateau region, Deep-Sea Res.Part I-Oceanographic Research Papers, 56, 963–973, 2009.

Martin, A. P.: Phytoplankton patchiness: the role of lateral stirring and mixing, Prog. Oceanogr., 57, 125–174, 2003.

Martin, A. P. and Pondaven, P.: On estimates for the vertical nitrate flux due to eddy pumping, J. Geophys. Res.-Oceans, 108, 3359, doi:10.1029/2003JC001841, 2003.

Martin, A. P. and Richards, K. J.: Mechanisms for vertical nutrient transport within a North Atlantic mesoscale eddy, Deep-Sea Res. Part II-Topical Studies In Oceanography, 48, 757–773, 2001.

McKiver, W. J. and Neufeld, Z.: Influence of turbulent advection on a phytoplankton ecosystem with nonuniform carrying capacity, Phys. Rev. E, 79, 061902, 2009.

McKiver, W., Neufeld, Z., and Scheuring, I.: Plankton bloom controlled by horizontal stirring, Nonlin. Processes Geophys., 16, 623–630, doi:10.5194/npg-16-623-2009, 2009.

Okubo, A.: Horizontal Dispersion Of Floatable Particles In Vicinity Of Velocity Singularities Such As Convergences, Deep-Sea Res., 17, 445, 1970.

Okubo, A.: Oceanic Diffusion Diagrams, Deep-Sea Res., 18, 789, 1971.

Pal, S., Chatterjee, S., Das, K. P., and Chattopadhyay, J.: Role of competition in phytoplankton population for the occurrence and control of plankton bloom in the presence of environmental fluctuations, Ecol. Model., 220, 96–110, 2009.

Pasquero, C., Bracco, A., and Provenzale, A.: Impact of the spatiotemporal variability of the nutrient flux on primary productivity in the ocean, J. Geophys. Res.-Oceans, 110, C07005, doi:10.1029/2004JC002738, 2005.

Paterson, H. L., Feng, M., Waite, A. M., Gomis, D., Beckley, L. E., Holliday, D., and Thompson, P. A.: Physical and chemical signatures of a developing anticyclonic eddy in the Leeuwin Current, eastern Indian Ocean, J. Geophys. Res.-Oceans, 113, C07049, doi:10.1029/2007JC004707, 2008.

Pérez-Muñuzuri, V. and Huhn, F.: The role of mesoscale eddies time and length scales on phytoplankton production, Nonlin. Processes Geophys., 17, 177–186, doi:10.5194/npg-17-177-2010, 2010.

Perruche, C., Riviere, P., Pondaven, P., and Carton, X.: Phytoplankton competition and coexistence: Intrinsic ecosystem dynamics and impact of vertical mixing, J. Marine Syst., 81, 99–111, 2010.

Richards, K. J. and Brentnall, S. J.: The impact of diffusion and stirring on the dynamics of interacting populations, J. Theor. Biol., 238, 340–347, 2006.

Rossi, V., López, C., Sudre, J., Hernández-García, E., and Garcon, V.: Comparative study of mixing and biological activity of the Benguela and Canary upwelling systems, Geophys. Res. Lett., 35, L11602, doi:10.1029/2008GL033610, 2008.

Sandulescu, M., Hernández-García, E., López, C., and Feudel, U.: Kinematic studies of transport across an island wake, with application to the Canary islands, Tlus Series A-Dynamic Meteorology And Oceanography, 58, 605–615, 2006.

Sandulescu, M., López, C., Hernández-García, E., and Feudel, U.: Plankton blooms in vortices: the role of biological and hydrodynamic timescales, Nonlin. Processes Geophys., 14, 443–454, doi:10.5194/npg-14-443-2007, 2007.

Sandulescu, M., López, C., Hernández-García, E., and Feudel, U.: Biological activity in the wake of an island close to a coastal upwelling, Ecological Complexity, 5, 228–237, 2008.

Scheuring, I., Károlyi, G., Toroczkai, Z., Tél, T., and Péntek, A.: Competing populations in flows with chaotic mixing, Theor. Popul. Biol., 63, 77–90, 2003.

Shea, K., Roxburgh, S. H., and Rauschert, E. S. J.: Moving from

pattern to process: coexistence mechanisms under intermediate disturbance regimes, Ecology Letters, 7, 491–508, 2004.

Steele, J. H. and Henderson, E. W.: A Simple Plankton Model, American Naturalist, 117, 676–691, 1981.

Strain, J.: Semi-Lagrangian methods for level set equations, J. Comput. Phys., 151, 498–533, 1999.

Strain, J.: A fast modular semi-Lagrangian method for moving interfaces, J. Comput. Phys., 161, 512–536, 2000.

Tél, T., de Moura, A., Grebogi, C., and Károlyi, G.: Chemical and biological activity in open flows: A dynamical system approach, Physics Reports-Review Section Of Physics Letters, 413, 91–196, 2005.

Weiss, J.: The Dynamics Of Enstrophy Transfer In 2-Dimensional Hydrodynamics, Physica D, 48, 273–294, 1991.